THE JOURNAL OF PHYSICAL CHEMISTRY C

pubs.acs.org/JPCC Article

# Dehydration Pathway of $CoF_2·4H_2O$ Revisited by Integrated ex Situ and in Situ Calorimetric and Structural Studies

Cody B. Cockreham, Xianghui Zhang, Vitaliy G. Goncharov, Xiaofeng Guo, Hongwu Xu, and Di Wu*

Cite This: J. Phys. Chem. C 2020, 124, 3551−3556 Read Online

ACCESS | Metrics & More | Article Recommendations

**ABSTRACT:** Cobalt(II) fluoride ($\alpha$-$CoF_2$) has potential for application as a high-performance electrode material in lithium-ion batteries. $\alpha$-$CoF_2$ is synthesized by the thermal heat treatment of $CoF_2·4H_2O$, commonly synthesized in an aqueous environment. There exists disagreement in the literature upon the mechanism, intermediate hydration states, and temperatures of the reaction. Here, we resolve this discontinuity by using integrated structural, thermogravimetric, and calorimetric analyses to elucidate the dehydration pathway of $CoF_2·4H_2O$ in both ex situ and in situ experimental conditions. Specifically, the decomposition of $CoF_2·4H_2O$ to $\alpha$-$CoF_2$ has been investigated using isothermal thermogravimetry (ex situ TG), thermogravimetry (TG)−differential scanning calorimetry (DSC), kinetic analysis, and ex situ and in situ X-ray diffraction (XRD). We deduce that in two irreversible steps $CoF_2·4H_2O$ completely decomposes into $\alpha$-$CoF_2$, with an amorphous intermediary phase of $CoF_2·0.5H_2O$. Under DSC conditions with a heating rate of 10 °C/min, $CoF_2·4H_2O$ dehydrates to $CoF_2·0.5H_2O$ from 80 to 175 °C, and further dehydration between 175 and 300 °C leads to $\alpha$-$CoF_2$. The $\alpha$-$CoF_2$ phase remains stable up to the highest temperature recorded, 400 °C.

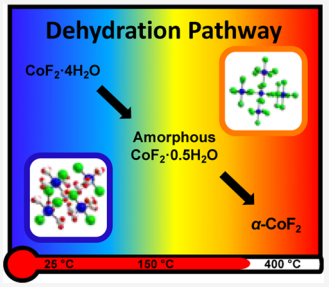


## INTRODUCTION

In the face of climate change, electric vehicles offer a significant reduction in carbon emissions over traditional transportation.[1] To enable commercially feasible and competitive electric vehicles, electrode materials with higher energy density are needed.[2] Transition metal fluorides have potential as lithium-ion battery cathode materials due to their high specific capacities.[2,3] Transition metal fluorides commonly exhibit multiple hydration states which can strongly affect their electrochemical performance.[4] As research continues into transition metal fluorides as electrode materials, it is important to examine not only the electrochemical properties of each of their hydration states but also the phase evolution and stability for better design and processing.

$CoF_2$ ($\alpha$-$CoF_2$) has recently received interest for application as an electrode material for energy storage[5−12] due to its high theoretical capacity (553 mA·h/g).[7] For optimal Li-ion insertion and greater performance, $CoF_2$ is employed as nanoparticles[5,6,8,12] or nanostructured hybrids[13] to increase its reactive surface area. One common strategy to create these nanostructures is by synthesis of $CoF_2·4H_2O$ in an aqueous environment followed by heat treatment to remove the waters of crystallization to form $\alpha$-$CoF_2$ (see Figure 1).[5,13] To best enable the controllable synthesis of $\alpha$-$CoF_2$ materials from $CoF_2·4H_2O$, it is important to understand the mechanisms of crystalline water loss.

Previous studies of the thermal decomposition of $CoF_2·4H_2O$ to the anhydrous $\alpha$-$CoF_2$ have produced a considerable disagreement in the mechanism and temperature ranges of decomposition. Moreover, ex situ and in situ analyses usually

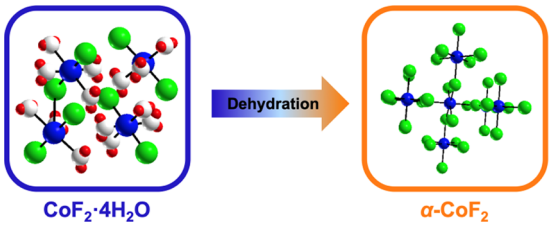


**Figure 1.** Crystal structures of $CoF_2·4H_2O$ and $\alpha$-$CoF_2$, cobalt in blue, fluoride in green, oxygen in white, and hydrogen in red.

lead to different conclusions. In 2008, Berdonosov et al., using thermogravimetric analysis (TGA), reported a three-step mechanism in which no water loss was seen below 120 °C, followed by the loss of about three water molecules to $CoF_2·0.9H_2O$ up to 310 °C and the loss of about one-half a water molecule to $CoF_2·0.4H_2O$ up to 440 °C, and finally, complete loss of crystalline water at 500 °C.[14] In 2016, Nasriddinov et al., using nonequilibrium and equilibrium tensiometry with a membrane null manometer, reported a two-step decomposition mechanism including dehydration to the intermediate $CoF_2·H_2O$ at 72 °C and complete dehydration at 107 °C.[15] Most recently, in 2018, using thermogravimetry (TG) coupled with differential scanning calorimetry (DSC), Khan et al.

Received: August 27, 2019
Revised: December 26, 2019
Published: December 31, 2019






https://dx.doi.org/10.1021/acs.jpcc.9b08175
J. Phys. Chem. C 2020, 124, 3551−3556

reported a single-step mechanism, reporting complete loss of crystalline water at 110 °C and no subsequent phase transition up to 525 °C.[5]

To effectively dehydrate $CoF_2·4H_2O$ and take advantage of $\alpha$-$CoF_2$'s potential as an electrode material, it is essential to identify each stage of the structural and compositional evolutions of $CoF_2·4H_2O$ under programmed thermal treatment. Here, using integrated structural, both ex situ and in situ, thermogravimetric, kinetic, and calorimetric analyses, we determine the decomposition stages of $CoF_2·4H_2O$. Our results strongly suggest a previously unreported two-step irreversible dehydration pathway with the presence of an amorphous intermediate phase.

## EXPERIMENTAL METHODS

$CoF_2·4H_2O$ was purchased from Sigma-Aldrich (99.99% purity). The powder had large grain sizes similar to pellets so was ground for 5 min prior to investigation to promote even heating. Thermogravimetry−differential scanning calorimetry (TG−DSC) analyses were performed simultaneously via a Netzsch STA 449 F5 Jupiter. The derivative of the TG and DSC curves was taken yielding derivative thermogravimetric analysis (DTG) and derivative differential scanning calorimetry (DDSC) curves. The measurements were carried out with heating rates of 5, 10, 15, and 20 °C/min up to 400 °C under a nitrogen flow rate of 50 mL/min. Isothermal thermogravimetric measurements, ex situ TG, were performed by weighing ∼100 mg sample of $CoF_2·4H_2O$ before and after isothermal heat treatment using a tube furnace in an argon atmosphere at a heating rate of 10 °C/min to the desired temperature followed by thermal treatment for 3 h. The sample was then gradually cooled to room temperature. The structural evolution from heat treatment was characterized by both ex situ and in situ powder X-ray diffraction (XRD). XRD data were obtained using a Rigaku Smartlab with Cu K$\alpha$ radiation ($k$ = 1.5406 Å) coupled with an Anton Paar XRK 900 furnace operated at a scan rate of 4°/min with a heating rate of 10 °C/min under 50 mL/min of argon with hold times of 5 min and 1 h. PDF database references were used to identify the phases of $CoF_2·4H_2O$, PDF-Card No. 00-025-0243, and $\alpha$-$CoF_2$, PDF-Card No. 01-071-1969. Scanning electron microscopy (SEM) was performed using a Tescan Vega3 operated at 20 kV and 72 $\mu$A.

Kinetic analysis was performed using the Ozawa−Flynn−Wall model-free method by using the nonisothermal thermogravimetric curves at different heating rates to draw isoconversional lines with which activation energy was found. The pre-exponential factor was estimated by assuming a first-order decomposition reaction (A → B + C). This method and a correction to the activation energy has been presented in great detail previously by Opfermann and colleagues.[16,17] Since the approach used here is identical to theirs, we choose not to expand the details in this paper.

## RESULTS

Thermogravimetric (TG) and the derivative thermogravimetric (DTG) curves of $CoF_2·4H_2O$ are presented in Figure 2a. Two decomposition stages are observed. First, the majority of water weight loss (−37 wt % for 10 °C/min) takes place rapidly. Subsequently, a subtle weight loss (−5 wt % for 10 °C/min) occurs gradually. Above 300 °C, no appreciable mass loss is seen. Accordingly, a singular sharp DTG peak implies a simple decomposition event. The second weight-loss event, being much more gradual and less significant, is not obvious. Weight loss from ex situ TG, 3 h at a particular temperature, is plotted in Figure 2b with the nonisothermal TG. Mirroring the isothermal TG curve, the majority of weight loss occurs from 50 to 100 °C with continued mass loss as temperature increases. The partial and total decomposition of $CoF_2·4H_2O$ lead to two nonisothermal TG weight-loss steps of −39 and −4 wt % at 175 and 300 °C with a heating rate of 10 °C/min. These two losses of crystalline water were recorded at 90 °C (−37 wt %) and 200 °C (−42 wt %) in the ex situ TG. Notably, compared with the nonisothermal TG curves, there is a significant left shift for the weight-loss plot of ex situ TG.

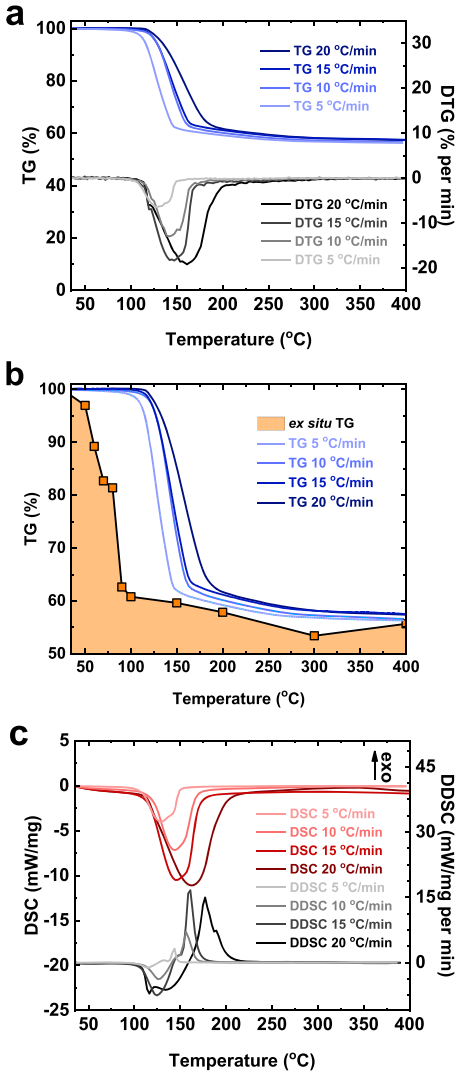


**Figure 2.** (a) Thermogravimetric and derivative thermogravimetric analysis (TG−DTG), (b) ex situ TG, and (c) differential scanning calorimetry and derivative differential scanning calorimetry (DSC−DDSC) curves of $CoF_2·4H_2O$ decomposition.

Differential scanning calorimetric (DSC) and the derivative differential scanning calorimetric (DDSC) curves are shown in Figure 2c. The DSC curve presents a sharp endothermic event corresponding to the loss of the waters of crystallization within $CoF_2·4H_2O$ and a low magnitude endothermic shoulder reflecting the second stage of minor loss of crystalline water. Integration of the DSC curve gives an average enthalpy of complete dehydration, from $CoF_2·4H_2O$ to $\alpha$-$CoF_2$, of 24.0


https://dx.doi.org/10.1021/acs.jpcc.9b08175
J. Phys. Chem. C 2020, 124, 3551−3556

kJ/mol of $H_2O$. The low magnitude of average enthalpy of dehydration strongly suggest loosely associated molecular water within the lattice of $CoF_2{\cdot}4H_2O$, which is energetically similar to what we observed for water confined within zeolites and on hydrophobic surfaces.[18−21] The corresponding DDSC profile appears to show one major endothermic event corresponding to an abrupt phase transition. However, its response curve is asymmetric and sharper than the initial endothermic curve implying a hidden, low magnitude second endothermic event.

The TG−DSC curves and DTG−DDSC curve peaks experience a shift toward higher temperatures as the heating rate increases. There is an increase in areas within the DSC and DDSC curves as the heating rate increases. Such phenomena, commonly seen in dehydration processes, indicate kinetic and transport limitations due to the nature of dynamic heating.[22,23] Decomposition chemical reactions, like all chemical reactions, take place over a period of time, because each decomposition step depends directly on the heating rate in a nonisothermal experiment. More explicitly, as the heating rate increases, at any given temperature during the reaction, the amount of unreacted and reacting hydrates increases and the transporting water vapor is yet to exit the material.[22,23] The phenomenon observed in this study is very similar to that of $CuSO_4{\cdot}5H_2O$ dehydration.[22]

To use the Ozawa−Flynn−Wall model-free method to kinetically analyze the nonisothermal thermogravimetric curves, isoconversional lines were drawn to determine the activation energies from the slope of each. Figure 3 presents a

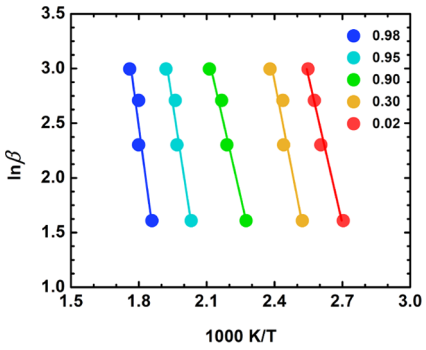


**Figure 3.** Ozawa−Flynn−Wall isoconversional lines for select conversions, where $T$ is the temperature (K) and $\beta$ is the heating rate (K/min).

representative group of isoconversional lines from a range of $\alpha$ = 0.02 to 0.98 ($\alpha$ being conversion). In Figure 4, the determined activation energies and estimated pre-exponential factors are plotted as a function of conversion $\alpha$. Pre-exponential factors are estimated using a first-order decomposition reaction model. In the case of only one reaction occurring, it is expected that the activation energy is independent of conversion. Three distinct regions of kinetic action are inferred from the two changes in activation energy and the pre-exponential factor. According to the kinetic analysis, the decomposition pathway appears to occur stagewise with at least two steps, Step 1: from $CoF_2{\cdot}4H_2O \rightarrow CoF_2{\cdot}0.5H_2O$ followed by Step 2: $CoF_2{\cdot}0.5H_2O \rightarrow \alpha$-$CoF_2$. Specifically, the initial activation energy of $CoF_2{\cdot}4H_2O$ dehydration is about 69 kJ/mol ($\ln A$ = 18), similar in magnitude to what has been reported for the decomposition of $CuSO_4{\cdot}5H_2O$ (75 kJ/mol). Subsequently, as the mass loss

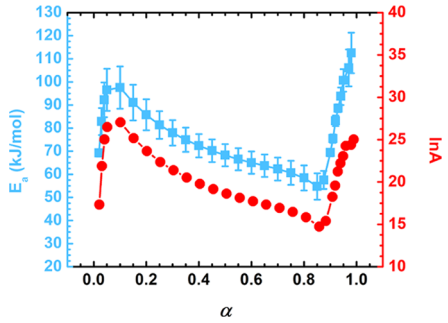


**Figure 4.** $E_a$ denotes the activation energy (kJ/mol) and $A$ represents the pre-exponential factor (1/s), presented as a function of conversion ($\alpha$).

increases, the activation energy switches abruptly to ∼98 kJ/mol ($\ln A$ = ∼28) and the average activation energy of this region is about 70 kJ/mol. At the conclusion of the thermal analysis, the activation energy experiences a sharp increase to 112 kJ/mol, at which $\ln A$ = 26.

Ex situ XRD patterns of $CoF_2{\cdot}4H_2O$ under heat treatment are shown in Figure 5a. When treated isothermally, $CoF_2{\cdot}$

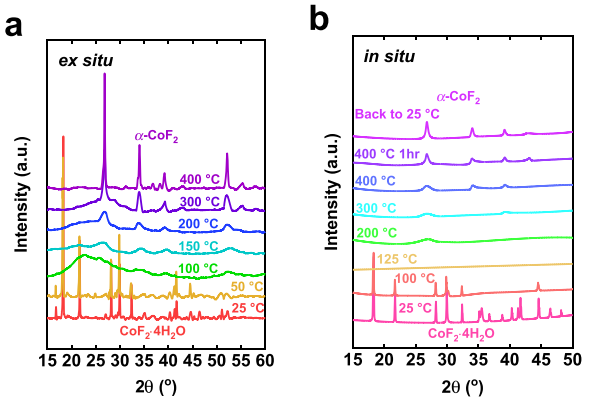


**Figure 5.** (a) Ex situ and (b) in situ X-ray diffraction (XRD) patterns of $CoF_2{\cdot}4H_2O$ as a function of temperature.

$4H_2O$ decomposition is witnessed at 100 °C, at which an amorphous intermediate phase ($CoF_2{\cdot}0.5H_2O$) is observed. Between 150 and 400 °C, $\alpha$-$CoF_2$'s patterns are resolved. $\alpha$-$CoF_2$ exhibits good thermal stability at 400 °C, evidenced by sharp representative peaks. In situ XRD patterns of $CoF_2{\cdot}4H_2O$ are shown in Figure 5b. The difference in signal-to-noise ratio between ex situ and in situ techniques is due to the differences caused by using the furnace apparatus in the in situ experiments. Generally, the ex situ and in situ XRD patterns share the same trend. Amorphization of $CoF_2{\cdot}4H_2O$ was observed at 125 °C. Subsequently, $\alpha$-$CoF_2$'s representative peak at ∼27° appears after 1 h at 200 °C, and its pattern is not very well-resolved until 400 °C. Heated dynamically in the DSC experiments with shorter hold times accounts for the phase transition lag seen in in situ versus ex situ investigation.

To illustrate the phase evolutions, the representative peak intensities, $CoF_2{\cdot}4H_2O$ at ∼16°, $CoF_2{\cdot}0.5H_2O$ using the baseline intensity, and $\alpha$-$CoF_2$ at ∼27°, of ex situ and in situ XRD data of each phase are plotted as a function of temperature (see Figure 6a,b). Generally, both ex situ and in situ data boast of a very similar trend. As $CoF_2{\cdot}4H_2O$ undergoes decomposition at 50 °C and above, the intensity at


https://dx.doi.org/10.1021/acs.jpcc.9b08175
J. Phys. Chem. C 2020, 124, 3551−3556

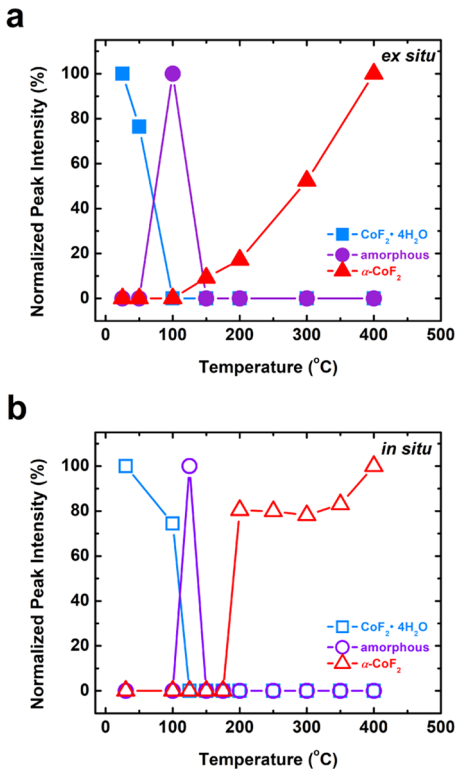


**Figure 6.** Normalized peak intensities of (a) ex situ (isothermally treated) and (b) in situ from X-ray diffraction (XRD) data of $CoF_2 \cdot 4H_2O$. The normalized peak intensities were calculated by the intensity of each representative peak: intensity of the strongest peak × 100%.

~16° decreases significantly, which suggests abrupt initiation of transition to an amorphous phase. The intermediate amorphous phase remains with low peak intensity until 200 °C followed by $\alpha$-$CoF_2$'s representative peak (at ~27°) intensity, which emerges and increases as temperature increases.

Visually, there is an abrupt phase transition observed in the normalized peak intensities of the in situ XRD curve of $\alpha$-$CoF_2$ compared to the sample analyzed in the ex situ experiment. This is because the sample analyzed by in situ XRD, which experienced effectively more heating time than the sample in ex situ thermal treatment, only showed eventual phase transition at temperatures higher than 200 °C, before which the sample is essentially in metastable states away from equilibrium due to the fast heating rate at 10 °C/min and holding time (5 + 9 min). In contrast, the normalized peak intensities of ex situ XRD data reflect equilibrated phases treated for 3 h at each temperature isothermally.

The morphological evolution from room temperature $CoF_2 \cdot 4H_2O$ to amorphous $CoF_2 \cdot 0.5H_2O$ at 100 °C (am-$CoF_2 \cdot 0.5H_2O$) to $\alpha$-$CoF_2$ at 400 °C is presented in the SEM images in Figure 7. At room temperature, the surface of bulk $CoF_2 \cdot 4H_2O$ is relatively smooth (Figure 7a,b). As temperature increases to 100 °C (Figure 7c,d), little holes and cracks emerge on the surface of am-$CoF_2$, which are likely due to dehydration and subsequent transport phenomena of the water vapor from the interior of the material. At 400 °C, to minimize the overall energy, sintering and formation of solid−solid interfaces among the $\alpha$-$CoF_2$ nanograins are observed (see Figure 7e,f).

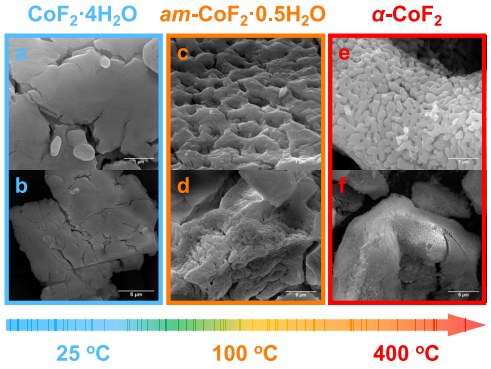


**Figure 7.** Scanning electron microscopy images (SEM) of ex situ isothermally treated $CoF_2 \cdot 4H_2O$ at room temperature with bar scales at (a) 1 $\mu$m and (b) 5 $\mu$m, 100 °C with bar scales at (c) 1 $\mu$m and (d) 5 $\mu$m, and 400 °C with bar scales at (e) 1 $\mu$m and (f) 5 $\mu$m. Here, "am-$CoF_2 \cdot 0.5H_2O$" denotes the amorphous cobalt fluoride hydrate intermediate phase as observed in Figure 5a at 100 °C. The scale bars are 1 $\mu$m for (a)−(c) and 5 $\mu$m for (d)−(f).

## DISCUSSION

The kinetic analysis indicates three distinct activation energies. The first two correspond to two weight-loss events from decomposition reactions seen in the thermogravimetric (TG−DTG) and energetic (DSC−DDSC) analyses and are in agreement with the structural analysis (XRD) that shows the formation of an intermediate amorphous $CoF_2 \cdot 0.5H_2O$ phase and subsequently the $\alpha$-$CoF_2$ phase. The third activation energy can be attributed to sintering of the nanograins with solid−solid interfaces expected to occur during decomposition as seen in the morphological analysis in Figure 7e,f. Corresponding well with the weight loss of the thermogravimetric steps reported by the TG and ex situ TG weight loss (−39/−37 and −43/−42 wt %, respectively) is the theoretical weight loss for partial decomposition to $CoF_2 \cdot 0.5H_2O$, −37 wt %, and the total decomposition to $\alpha$-$CoF_2$, −43 wt %. The kinetic, thermal, and structural analyses suggest the following irreversible decomposition mechanism

$$\text{Step 1: } CoF_2 \cdot 4H_2O \rightarrow CoF_2 \cdot 0.5H_2O + 3.5H_2O$$

$$\text{Step 2: } CoF_2 \cdot 0.5H_2O \rightarrow \alpha - CoF_2 + 0.5H_2O$$

Because $CoF_2 \cdot 0.5H_2O$ exhibits thermal stability from approximately 100 to 300 °C, and because dehydration of $CoF_2 \cdot 0.5H_2O$ to $\alpha$-$CoF_2$ represents only ~5% of the total observed water loss, the dehydration pathway of $CoF_2 \cdot 4H_2O$ could easily be mistakenly identified as direct decomposition from $CoF_2 \cdot 4H_2O$ to $\alpha$-$CoF_2$.[5] Interestingly, the intermediate hydration product observed here is amorphous, lacking long-range order (see Figure 5). The final decomposition product, $\alpha$-$CoF_2$, has well-resolved crystallinity and is structurally intact and thermally stable at 400 °C, supported by both ex situ and in situ XRD data. At a particular temperature, the sample analyzed using ex situ methods (ex situ TG and ex situ XRD) tends to have better-defined phases at each temperature as seen by the more intense peaks compared to baseline (see Figure 5). This is because of the difference in heating rate and equilibrium time applied in the in situ versus ex situ thermogravimetric, calorimetric, and structural experiments. The ex situ TG and XRD demonstrate that the dehydrated phases are stable in the air upon cooling so the decomposition of $CoF_2 \cdot 4H_2O$ and $CoF_2 \cdot 0.5H_2O$ is irreversible under the time


https://dx.doi.org/10.1021/acs.jpcc.9b08175
J. Phys. Chem. C 2020, 124, 3551−3556

constraints and conditions of these experiments. In summary, our analysis shows a two-stage irreversible dehydration pathway with an intermediate phase of $CoF_2{\cdot}0.5H_2O$.

Generally, our analysis is in agreement with the TG−DSC data reported by Khan et al., yet we have a distinctly different interpretation.[5] Since the weight loss and energetic difference between $CoF_2{\cdot}0.5H_2O$ and $\alpha$-$CoF_2$ are both small in magnitudes compared with the large mass change and heat effects of the initial $CoF_2{\cdot}4H_2O$ to $CoF_2{\cdot}0.5H_2O$ reaction, Khan et al. might overlook this stable intermediate phase and considered it to be a product of kinetic or mass transport resistance. The existence of a $CoF_2{\cdot}0.5H_2O$ to $\alpha$-$CoF_2$ reaction and a stable intermediate $CoF_2{\cdot}0.5H_2O$ phase is clearly identified by our integrated kinetic analysis and structural investigation. Although Berdonosov et al. using a thermogravimetric method reported $CoF_2{\cdot}0.9H_2O$, not seen here, they described the existence of a similar intermediate phase of $CoF_2{\cdot}0.4H_2O$.[14] It is possible that Berdonosov et al.'s $CoF_2{\cdot}0.4H_2O$ might actually be the $CoF_2{\cdot}0.5H_2O$ phase that we have identified here. Nevertheless, without the technical specifications of their experimental thermogravimetric device, analytical method, the initial purity or source of cobalt nitrate and cobalt sulfate used, we are not able to be convinced. Moreover, although it was claimed that the samples were characterized by XRD and the fluoride content was measured by potentiometry, no experimental data were presented. Nasriddinov et al. concluded that the dehydration process of $CoF_2{\cdot}4H_2O$ consists of two steps.[15] However, similarly, no experimental data were presented to support their conclusion.[15] Here, we have resolved the disagreement in the literature by thorough reexamination of the thermal decomposition process of $CoF_2{\cdot}4H_2O$ using a multitude ex situ and in situ studies using integrated calorimetric and structural analyses.

## CONCLUSIONS

By integrating ex situ and in situ XRD with coupled thermogravimetric and calorimetric analyses, we have elucidated the decomposition mechanism for $CoF_2{\cdot}4H_2O$. Illuminating the pathway of dehydration for $CoF_2{\cdot}4H_2O$ allows better phase control during decomposition to $\alpha$-$CoF_2$. $CoF_2{\cdot}4H_2O$ decomposes irreversibly in two steps, from $CoF_2{\cdot}4H_2O$ to $CoF_2{\cdot}0.5H_2O$ to $\alpha$-$CoF_2$. Using ex situ and in situ XRD, we demonstrate that the $CoF_2{\cdot}0.5H_2O$ intermediate phase is amorphous. $\alpha$-$CoF_2$ shows the most well-defined crystallinity when treated up to 400 °C. The variations in the heating rate and equilibrium time in the in situ and ex situ thermogravimetric, calorimetric, and structural experiments lead to a shifted decomposition profile as a function of temperature. For thermal treatment of $CoF_2{\cdot}4H_2O$ in the synthesis of $\alpha$-$CoF_2$, we recommend heating to 400 °C regardless of the heating rate. Furthermore, with unexplored electrochemical performance, the $CoF_2{\cdot}0.5H_2O$ amorphous phase may serve as a viable alternative to $CoF_2{\cdot}4H_2O$ and $\alpha$-$CoF_2$ as an electrode material.

## AUTHOR INFORMATION


### Corresponding Author

**Di Wu** − *Alexandra Navrotsky Institute for Experimental Thermodynamics, Voiland School of Chemical Engineering and Bioengineering, Department of Chemistry, and Materials Science and Engineering, Washington State University, Pullman, Washington 99164, United States;* orcid.org/0000-0001-6879-321X; Email: d.wu@wsu.edu

### Authors

**Cody B. Cockreham** − *Alexandra Navrotsky Institute for Experimental Thermodynamics and Voiland School of Chemical Engineering and Bioengineering, Washington State University, Pullman, Washington 99164, United States; Earth and Environmental Sciences Division, Los Alamos National Laboratory, Los Alamos, New Mexico 87545, United States*

**Xianghui Zhang** − *Alexandra Navrotsky Institute for Experimental Thermodynamics and Voiland School of Chemical Engineering and Bioengineering, Washington State University, Pullman, Washington 99164, United States*

**Vitaliy G. Goncharov** − *Alexandra Navrotsky Institute for Experimental Thermodynamics and Department of Chemistry, Washington State University, Pullman, Washington 99164, United States; Earth and Environmental Sciences Division, Los Alamos National Laboratory, Los Alamos, New Mexico 87545, United States*

**Xiaofeng Guo** − *Alexandra Navrotsky Institute for Experimental Thermodynamics, Department of Chemistry, and Materials Science and Engineering, Washington State University, Pullman, Washington 99164, United States;* orcid.org/0000-0003-3129-493X

**Hongwu Xu** − *Earth and Environmental Sciences Division, Los Alamos National Laboratory, Los Alamos, New Mexico 87545, United States*

Complete contact information is available at: https://pubs.acs.org/10.1021/acs.jpcc.9b08175


### Notes

The authors declare no competing financial interest.

## ACKNOWLEDGMENTS

This work was supported by the institutional funds from the Gene and Linda Voiland School of Chemical Engineering and Bioengineering at Washington State University. D.W. acknowledges the fund of Alexandra Navrotsky Institute for Experimental Thermodynamics. C.B.C. received support from the Achievement Rewards for College Scientists (ARCS) Fellowship from the ARCS Seattle Chapter and the Natural Resource Conservation Fund (NRCEF) through the Office of Research at WSU. X.Z. is supported by the Chambroad Distinguished Fellowship.

## REFERENCES


(1) Holdway, A. R.; Williams, A. R.; Inderwildi, O. R.; King, D. A. Indirect Emissions from Electric Vehicles: Emissions from Electricity Generation. *Energy Environ. Sci.* **2010**, *3*, 1825−1832.

(2) Andre, D.; Kim, S.-J.; Lamp, P.; Lux, S. F.; Maglia, F.; Paschos, O.; Stiaszny, B. Future Generations of Cathode Materials: An Automotive Industry Perspective. *J. Mater. Chem. A* **2015**, *3*, 6709−6732.

(3) Amatucci, G. G.; Pereira, N. Fluoride Based Electrode Materials for Advanced Energy Storage Devices. *J. Fluorine Chem.* **2007**, *128*, 243−262.

(4) Liu, L.; Guo, H.; Zhou, M.; Wei, Q.; Yang, Z.; Shu, H.; Yang, X.; Tan, J.; Yan, Z.; Wang, X. A Comparison among $FeF_3{\cdot}3H_2O$, $FeF_3{\cdot}0.33H_2O$ and $FeF_3$ Cathode Materials for Lithium Ion Batteries: Structural, Electrochemical, and Mechanism Studies. *J. Power Sources* **2013**, *238*, 501−515.

(5) Khan, J.; Ullah, H.; Sajjad, M.; Ali, A.; Thebo, K. H. Synthesis, Characterization and Electrochemical Performance of Cobalt Fluoride Nanoparticles by Reverse Micro-Emulsion Method. *Inorg. Chem. Commun.* **2018**, *98*, 132−140.

(6) Guan, Q.; Cheng, J.; Li, X.; Ni, W.; Wang, B. Porous $CoF_2$ Spheres Synthesized by a One-Pot Solvothermal Method as High Capacity Cathode Materials for Lithium-Ion Batteries. *Chin. J. Chem.* **2017**, *35*, 48−54.
(7) Armstrong, M. J.; Panneerselvam, A.; O'Regan, C.; Morris, M. A.; Holmes, J. D. Supercritical-Fluid Synthesis of $FeF_2$ and $CoF_2$ Li-Ion Conversion Materials. *J. Mater. Chem. A* **2013**, *1*, 10667−10676.
(8) Wang, X.; Gu, W.; Lee, J. T.; Nitta, N.; Benson, J.; Magasinski, A.; Schauer, M. W.; Yushin, G. Carbon Nanotube-$CoF_2$ Multifunctional Cathode for Lithium Ion Batteries: Effect of Electrolyte on Cycle Stability. *Small* **2015**, *11*, 5164−5173.
(9) Teng, Y. T.; Pramana, S. S.; Ding, J.; Wu, T.; Yazami, R. Investigation of the Conversion Mechanism of Nanosized $CoF_2$. *Electrochim. Acta* **2013**, *107*, 301−312.
(10) Li, H.; Balaya, P.; Maier, J. Li-Storage via Heterogeneous Reaction in Selected Binary Metal Fluorides and Oxides. *J. Electrochem. Soc.* **2004**, *151*, A1878.
(11) Fu, Z.-W.; Li, C.-L.; Liu, W.-Y.; Ma, J.; Wang, Y.; Qin, Q.-Z. Electrochemical Reaction of Lithium with Cobalt Fluoride Thin Film Electrode. *J. Electrochem. Soc.* **2005**, *152*, E50.
(12) Ma, R.; Zhou, Y.; Yao, L.; Liu, G.; Zhou, Z.; Lee, J. M.; Wang, J.; Liu, Q. Capacitive Behaviour of $MnF_2$ and $CoF_2$ Submicro/Nanoparticles Synthesized via a Mild Ionic Liquid-Assisted Route. *J. Power Sources* **2016**, *303*, 49−56.
(13) Chong, S.; Chen, Y.; Yan, W.; Guo, S.; Tan, Q.; Wu, Y.; Jiang, T.; Liu, Y. Suppressing Capacity Fading and Voltage Decay of Li-Rich Layered Cathode Material by a Surface Nano-Protective Layer of $CoF_2$ for Lithium-Ion Batteries. *J. Power Sources* **2016**, *332*, 230−239.
(14) Berdonosov, S. S.; Lebedev, V. Y.; Berdonosova, D. G.; Prokofiev, M. A.; Znamenskaya, I. V.; Melkhov, I. V.; Kharisov, B. I.; Mendez, U. O.; Kharissova, O. V. Influence of Microwave Treatment on the Dehydration of Crystallohydrates of Iron, Cobalt, and Nickel Fluorides. *J. Microwave Power Electromagn. Energy* **2007**, *42*, 15−20.
(15) Badalov, A. B.; Nasriddinov, S. K.; Islamova, M. S. Thermal stability and thermodynamic characteristics of crystalline hydrates of cobalt(II) fluoride. *Vestn. S.-Peterb. Univ., Ser. 4: Fiz., Khim.* **2018**, *5*, 435−442.
(16) Opfermann, J. Kinetic Analysis Using Multivariate Non-Linear Regression I. Basic Concepts. *J. Therm. Anal. Calorim.* **2000**, *60*, 641−658.
(17) Opfermann, J.; Kaisersberger, E. An Advantageous Variant of the Ozawa-Flynn-Wall Analysis. *Thermochim. Acta* **1992**, *203*, 167−175.
(18) Sun, H.; Wu, D.; Guo, X.; Shen, B.; Navrotsky, A. Energetics of Sodium-Calcium Exchanged Zeolite A. *Phys. Chem. Chem. Phys.* **2015**, *17*, 11198−11203.
(19) Sun, H.; Wu, D.; Liu, K.; Guo, X.; Navrotsky, A. Energetics of Alkali and Alkaline Earth Ion-Exchanged Zeolite A. *J. Phys. Chem. C* **2016**, *120*, 15251−15256.
(20) Wu, D.; Guo, X.; Sun, H.; Navrotsky, A. Energy Landscape of Water and Ethanol on Silica Surfaces. *J. Phys. Chem. C* **2015**, *119*, 15428−15433.
(21) Wu, D.; Guo, X.; Sun, H.; Navrotsky, A. Interplay of Confinement and Surface Energetics in the Interaction of Water with a Metal-Organic Framework. *J. Phys. Chem. C* **2016**, *120*, 7562−7567.
(22) Cheng, L.; Li, W.; Li, Y.; Yang, Y.; Li, Y.; Cheng, Y.; Song, D. Thermal Analysis and Decomposition Kinetics of the Dehydration of Copper Sulfate Pentahydrate. *J. Therm. Anal. Calorim.* **2019**, *135*, 2697−2703.
(23) Mianowski, A.; Baraniec-Mazurek, I.; Bigda, R. Some Remarks on Equilibrium State in Dynamic Condition. *J. Therm. Anal. Calorim.* **2012**, *107*, 1155−1165.


https://dx.doi.org/10.1021/acs.jpcc.9b08175
*J. Phys. Chem. C* 2020, 124, 3551−3556